SCIENCE CHINA
Physics, Mechanics & Astronomy

• Article •

April 2012 Vol.55 No.4: 671–683
doi: 10.1007/s11433-012-4680-2

Research on the transfers to Halo orbits from the view of invariant manifolds

XU Ming[1*], TAN Tian[2] & XU ShiJie[1]

[1] *Beijing University of Aeronautics and Astronautics, Beijing 100191, China;*
[2] *DFH Satellite Co. Ltd., Beijing 100094, China*

Received June 8, 2011; accepted September 20, 2011; published online March 8, 2012

This paper discusses the evolutions of invariant manifolds of Halo orbits by low-thrust and lunar gravity. The possibility of applying all these manifolds in designing low-thrust transfer, and the presence of single-impulse trajectories under lunar gravity are also explained. The relationship between invariant manifolds and the altitude of the perigee is investigated using a Poincaré map. Six types of single-impulse transfer trajectories are then attained from the geometry of the invariant manifolds. The evolutions of controlled manifolds are surveyed by the gradient law of Jacobi energy, and the following conclusions are drawn. First, the low thrust (acceleration or deceleration) near the libration point is very inefficient that the spacecraft free-flies along the invariant manifolds. The purpose is to increase its velocity and avoid stagnation near the libration point. Second, all controlled manifolds are captured because they lie inside the boundary of Earth's gravity trap in the configuration space. The evolutions of invariant manifolds under lunar gravity are indicated from the relationship between the lunar phasic angle and the altitude of the perigee. Third and last, most of the manifolds have preserved their topologies in the circular restricted three-body problem. However, the altitudes of the perigee of few manifolds are quite non-continuous, which can be used to generate single-impulse flyby trajectories.

libration point, Halo orbit, transfer trajectory, invariant manifolds, low thrust, lunar perturbation

PACS number(s): 95.10.Ce, 45.50.Pk, 45.50.Jf, 05.45.-a, 95.40.1s

Citation: Xu M, Tan T, Xu S J. Research on the transfers to Halo orbits from the view of invariant manifolds. Sci China-Phys Mech Astron, 2012, 55: 671–683, doi: 10.1007/s11433-012-4680-2

The theory of space manifolds dynamics has drawn increasing attention from astronautical scholars and industries worldwide. Some periodic solutions, such as Lagrange points and Halo orbits, have found important applications in deep-space missions since the ISEE-3 was successfully launched in 1978 [1,2]. Currently, there are several probes for missions involving libration points in the Sun-Earth/Moon system. Some spacecrafts, such as ISEE-3, Wind, SOHO, ACE, and Genesis, are located at EL_1 to survey solar wind. Other probes, such as MAP, are located around EL_2 to survey the outer space.

The transfer trajectories from their parking orbits around the Earth to Halo orbits are common focuses of research because Lagrange points and Halo orbits are encompassed by astrodynamics. Farquhar [3] is the first to study the transfer trajectories from the Earth to the Halo orbit. A shooting method is employed to generate the trajectories for the ISEE-3 mission by a number of iterations. Gómez [4] has investigated trajectories from the view of dynamical systems, and discovered that stable manifolds of Halo orbits display hyperbolic dynamical behaviors which are concluded to follow a heuristic methodology for designing the transfer trajectories from the Earth to the Halo orbit. Howell [5] has combined the theory of invariant manifolds with differential corrections to generate the transfer trajectories

*Corresponding author (email: xuming@buaa.edu.cn)

in the real Sun-Earth/Moon system, and indicated the relationship between the magnitudes of Halo orbits and the approaches of their invariant manifolds. Halo orbits with larger magnitudes may have invariant manifolds closer to Earth. Xu [6] has referred to the trajectories inserting the Halo orbit from the Earth's parking orbit only with an initial maneuver as single-impulse trajectories (SITs). Six types of SITs are obtained. Types A and B, which are adopted by the Wind and Genesis missions, are classified as direct transfer. On the other hand, types C, D, E, and F, which are always ignored by previous missions, are classified as indirect transfer.

The low-thrust propulsion and maneuver technology by planetary-gravity assist is considered significant advances in astronautical engineering [7,8] and has found many applications in designing the trajectories for Halo orbits in the Sun-Earth/Moon system. Both the SOHO and WIND spacecrafts employed flyby (or swingby) trajectories under lunar gravity. The distance between the Halo orbit and the Earth is four times greater than that between the Earth and the Moon. Therefore, the spacecraft has enough temporal and spatial manifolds to modify its flight directions to insert Halo orbit by lunar flyby. Howell [9] has constructed unperturbed trajectories from patched-conic illustrations. The construction is an initial guess to generate the real flyby trajectories in an ephemeris model from the iterative routine based on the pseudo-state theory. The trajectories employ low-thrust propulsion to perform gradient-type transfer to Halo orbit. The low thrust imposes continuous acceleration (or deceleration) on the right hand of differential equations. The dynamical topologies of the system from Hamiltonian to dissipative are also modified, and controlled gradient manifolds for Halo orbits are created. Ren [10] modified the endings of invariant manifolds in the geocentric flight of an escaping segment. The spacecraft is led to insert the invariant manifolds of Halo orbit after escaping from the Earth. However, Qin [11] has employed a solar sail to modify invariant manifolds and generate the transfer trajectories from the Earth to the Halo orbit.

The current paper presents the evolutions of the invariant manifolds of Halo orbits in the circular restricted three-body problem (CR3BP), and the spatial bi-circular model (SBCM). The possible application of these manifolds in designing low-thrust transferring trajectories, and the presence of single-impulse trajectories under lunar gravity are explained. The relationship between the manifolds and the altitude of the perigee is investigated using a Poincaré map. Six types of SITs are attained from the geometry of the invariant manifolds. The evolutions of the controlled manifolds are indicated by the gradient law of Jacobi energy, and the following conclusions are drawn. First, the low thrust (acceleration or deceleration) near the libration point is very inefficient that the spacecraft free-flies along the invariant manifolds to increase its velocity and avoid stagnation near the libration point. Second, all the controlled manifolds are captured because they lie inside the boundary of Earth's gravity trap in the configuration space. A turning on/off schedule for low-thrust propulsion is introduced for the controlled manifolds avoiding the stagnation on the libration points to measure the interception distance along the x axis. The evolutions of invariant manifolds under lunar gravity are indicated from the relationship between the lunar phasic angle as well as the altitudes of the perigee and perilune. Third and last, most of the manifolds have preserved their topologies in the CR3BP, which are used to generate the transfer trajectories from the Earth or the Moon to Halo orbits. However, the perigee altitudes of some manifolds are quite non-continuous, which can be used to generate the single-impulse flyby trajectories.

The present paper focuses on the evolutions of invariant manifolds of Halo orbit under low-thrust propulsion and lunar gravity. There are three main contributions: firstly, all invariant manifolds can be applied to design low-thrust transferring trajectories; secondly, there are remaining single-impulse trajectories preserved under lunar gravity; thirdly, trajectories can be constructed from ergodic surveys of the parameters of the phasic angles of Halo orbit, and the relative phases of the Sun, the Earth, and the Moon. These constructed trajectories simulate the real transfer trajectories to the Halo orbit in the ephemeris model from the iterative routine.

1 Dynamical system and Halo orbits

1.1 Coordinate frames defined in the dynamical system

Some coordinate frames referred to in the modeling are defined as follows. First is the Geocentric Inertial Coordinate System (GI). The origin is fixed at the geocenter. The x axis is along the intersecting line of the ecliptic and lunar orbital planes. The z axis is perpendicular to the lunar plane and accordant with the rotational direction of the Moon. The y axis is determined by the right-hand rule. For a spacecraft flying near the Earth, the coordinate system is a very close approximation of the real inertial reference frame.

Second is the Selenocentric Inertial Coordinate System (SI). The origin is fixed at selenocenter. All three axes are defined in the same way as those in the GI coordinate system. Obviously, the coordinate system is also a very close approximation of the real inertial reference frame for a spacecraft flying near the Moon.

Third is the Syzygy coordinate system of the Earth-Moon System (S_{E-M}). The origin is fixed at the centroid of the Earth-Moon system. The x axis points from the Earth to the Moon. The z axis is perpendicular to the lunar plane, and accordant with the rotational direction of the Moon. The y axis is determined by the right-hand rule.

Fourth is the Syzygy Coordinate System of Sun-Earth/Moon System (S_{S-E+M}). The origin is fixed at the centroid of

the Sun-Earth/Moon system. The x axis points from the Sun to the centroid of the Earth-Moon system. The z axis is perpendicular to the ecliptic plane, and accordant with the rotational direction of the Earth and Moon. The y axis is determined by the right-hand rule.

1.2 Circular restricted three-body problem

The Sun and Earth/Moon system move in near-circular orbits around their common center of mass. A massless spacecraft moves under the gravities of the Sun and Earth/Moon (the Earth and Moon are considered the small mass point). This relationship between the spacecraft, the Sun and Earth/Moon is referred to as CR3BP. To improve the efficiency and accuracy of calculation, we use normalized units (i.e., units of length, time, and mass) in CR3BP, as in $L_{\text{S–E+M}}$ = 1.4960×10^{11} m, $T_{\text{S–E+M}} = 2\pi$/year, and $M_{\text{S–E+M}} = 2 \times 10^{30}$ kg. The Hamiltonian for CR3BP is as follows:

$$H_0 = \frac{1}{2}\left(p_x^2 + p_y^2 + p_z^2\right) - xp_y + yp_x - \frac{1-\mu}{r_1} - \frac{\mu}{r_2}, \qquad (1)$$

where p_x , p_y , and p_z are the generalized momentums; and r_i (i = 1 and 2) are the distances from the spacecraft to the Sun , and the Earth/Moon system, respectively.

1.3 Halo orbits

Halo orbits bifurcating from the planar Lyapunov orbits are the periodic solutions of the CR3BP. Halo orbits are symmetrical to the plane x-z in the Syzygy reference frame. Determining the state of any point on a Halo orbit (with its period as T_{H}) only needs the magnitude A_x and the phase angle θ, as in the equation:

$$\boldsymbol{X} = \boldsymbol{\Gamma}\left(A_x, \theta\right) = \boldsymbol{H}\left(A_x, t\right),\ \theta \in \boldsymbol{R}/2\pi\boldsymbol{Z},\ t \in \boldsymbol{R}/T_{\text{H}}\boldsymbol{Z}, \qquad (2)$$

where $\boldsymbol{X}$ is the state variable of the dynamical system, $\boldsymbol{X} = \left[x \quad y \quad z \quad \dot{x} \quad \dot{y} \quad \dot{z}\right]^{\text{T}}$.

There is no analytical solution to the CR3BP due to its non-integrability. The equivalence relation is defined as:

$$\boldsymbol{X}_1 \sim \boldsymbol{X}_2 \Leftrightarrow \exists \tau, \boldsymbol{X}_2 = \boldsymbol{\varphi}_\tau\left(\boldsymbol{X}_1\right), \qquad (3)$$

where $\boldsymbol{\varphi}$ is the flow. Any point $\boldsymbol{X}_0$ can represent the whole flow from the equivalence relation of the time-independent Hamiltonian system. Hence, the numerical position and velocity on the point need to be iteratively achieved to gain knowledge on the Halo orbit.

If $\boldsymbol{X}_0$ is laid on the symmetry plane of Halo orbit, i.e., $\boldsymbol{X}_0 = \left[x_0 \quad 0 \quad z_0 \quad 0 \quad \dot{y}_0 \quad 0\right]^{\text{T}}$, the numerical algorithm for $\boldsymbol{X}_0$ is achieved.

Firstly, the approximate three-order analytical solution to the Halo orbit (called the Richardson Expansion [12], developed from the Lindstedt–Poincaré method) is employed to generate the approximation of $\boldsymbol{X}_0$.

Secondly, the approximation of $\boldsymbol{X}_0$ is taken as the initiation to integrate the dynamical equation describing CR3BP until the flow arrives at the symmetry plane. Consequently, the final value of the state variables is obtained as:

$$\boldsymbol{X}_f = \left[x_f \quad 0 \quad z_f \quad \dot{x}_f \quad \dot{y}_f \quad \dot{z}_f\right]^{\text{T}}.$$

Lastly, based on the Newton iteration, x_0 and $\dot{y}_0$ are required to gradually yield $\dot{x}_f$ and $\dot{z}_f$ close to zero:

$$\begin{cases} \delta\dot{x}_0 = \left(\boldsymbol{\Phi}_{41} - \dfrac{\boldsymbol{\Phi}_{21}\ddot{x}_f}{\dot{y}_f}\right)\delta x_0 + \left(\boldsymbol{\Phi}_{45} - \dfrac{\boldsymbol{\Phi}_{25}\ddot{x}_f}{\dot{y}_f}\right)\delta\dot{y}_0, \\ \delta\dot{z}_0 = \left(\boldsymbol{\Phi}_{61} - \dfrac{\boldsymbol{\Phi}_{21}\ddot{z}_f}{\dot{y}_f}\right)\delta x_0 + \left(\boldsymbol{\Phi}_{65} - \dfrac{\boldsymbol{\Phi}_{25}\ddot{z}_f}{\dot{y}_f}\right)\delta\dot{y}_0, \end{cases} \qquad (4)$$

where $\boldsymbol{\Phi}_{ij}$ is the element located in the i^{th} row and j^{th} column of the monodromy matrix $\boldsymbol{\Phi}$. Hence, 4–5 iterations are necessary to bring the position errors to less than 10km after a period.

The phasic angle of Halo orbit at EL_1 or EL_2 is defined by the equi-time interval $\tau = \left(i-1\right)/N, i = 1, ..., N,$ counting from the symmetry point and in the negative direction around the z axis, as depicted in Figure 1.

To analyze the stability of Halo orbits, we define the Poincaré map $\boldsymbol{P}\left(z\right)$ as:

$$\boldsymbol{P}\left(z\right) = \boldsymbol{\varphi}_{T_{\text{H}}}\left(z\right), \forall z \in \boldsymbol{\Gamma}\left(\theta\right). \qquad (5)$$

According to the dynamical theory of the Hamiltonian system, the differential matrix of $\boldsymbol{P}\left(z\right)$, $\boldsymbol{\Phi} = \boldsymbol{D}_z\boldsymbol{P}\left(z\right)$, is symplectic. The eigenvalues of $\boldsymbol{\Phi}$ are referred to as the characteristic exponents of the Poincaré map. Four eigenvalues lie on the unit circle, i.e., $\left|\lambda\right|_i = 1, i = 1, 2, 3, 4$, with two real eigenvalues $\lambda_{1,2} = 1,$ and two complex eigenvalues $\left|\lambda\right|_{3,4} = 1$. Other eigenvalues are both real with $\lambda_5 = \lambda_6^{-1} >$ 1, indicating the stability of Halo orbits.

The maximal real eigenvalue λ_5 is called the Floquet multiplier. This term connotes the deflection of the periodic orbit from its nominal trajectory under perturbations at the exponential rate of $\lambda_5 - 1$. Figure 2 reveals the relation between the magnitude A_x of Halo orbits and the function *ln* of the Floquet multiplier. From the view of stability, the Floquet multiplier may stay near 1. However, it causes the magnitude of Halo orbit to become too large to finish astronautical missions. For some cases, a smaller magnitude is preferred even at the cost of increased stationkeeping.

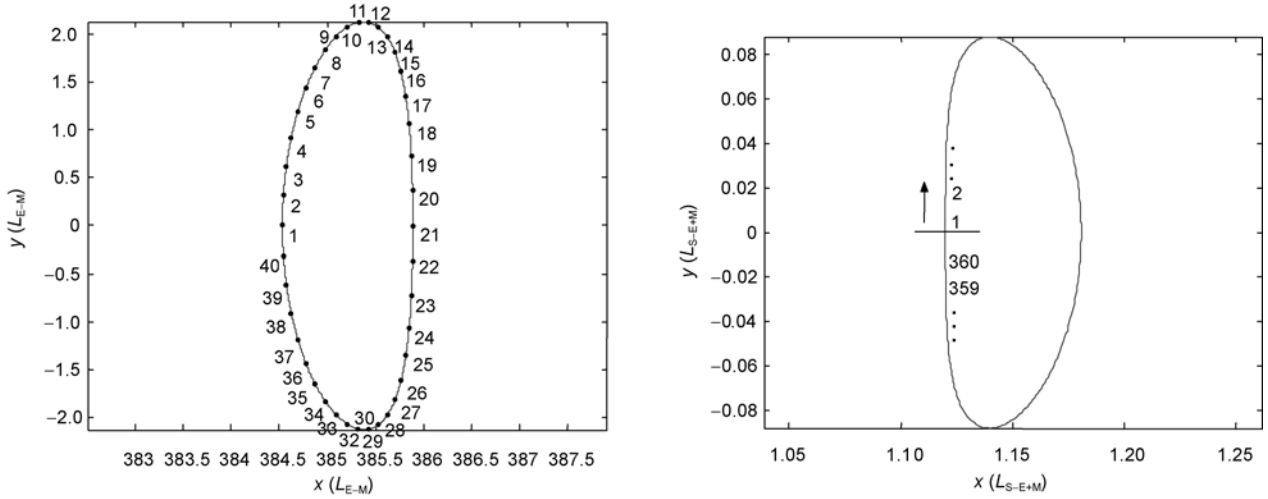

Figure 1 Phasic angle of the Halo orbit depicted in the *x*-*y* plane.

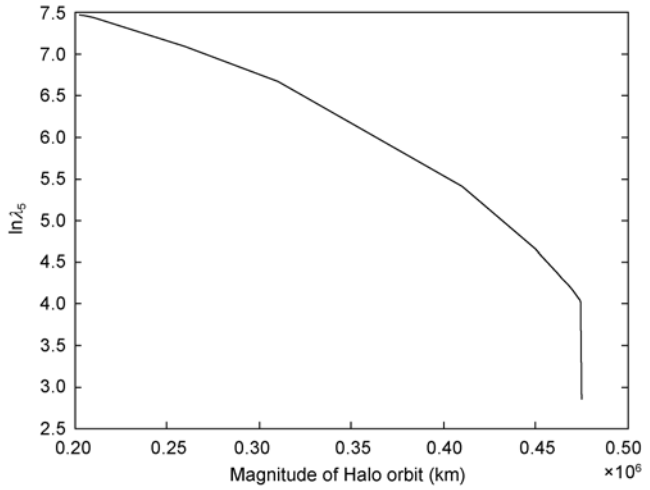

Figure 2 Relation between the magnitude A_x ($\times 10^6$ km) and the *ln* function of the floquet multiplier.

In the present paper, the magnitude of the Halo orbit at EL_1 is adopted as A_x=260000 km as the Genesis, with its Floquet multiplier as 1219.3, and its period as 5.8228 months. On the other hand, the magnitude of the Halo orbit at EL_2 is adopted as A_x = 350000 km, with its period as 5.8657 months.

1.4 Spatial Bi-circular model

The motions of the Sun, the Earth, and the Moon are the true solutions to a general three-body problem, which are too complicated for modeling and analysis. Hence, the SBCM is introduced as an approximate model for the general three-body problem, as shown in Figure 3. Accommodating the inclination between the lunar and ecliptic planes, the SBCM assumes the Earth and the Moon as one celestial body to implement two-body motion with respect to the Sun. The Sun's gravity is also assumed to have no influence on

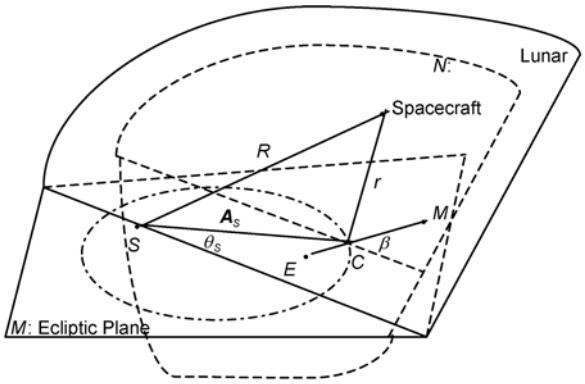

Figure 3 Profile of the SBCM Model.

the two-body motion between the Earth and Moon. Hence, the SBCM has a higher accuracy because the distance from the Sun to the Earth or the Moon is much longer than that between the Earth and the Moon. Consequently, the torque of the Sun's gravitation imposed on the Earth-Moon system can be ignored. However, the force acting from the Sun's gravitation on the centroid of the Earth/Moon system cannot be ignored.

In the real Sun-Earth/Moon system, the gravities of the Earth and the Moon impose short-term periodic perturbations onto the CR3BP describing the Sun-Earth/Moon system. The Sun's gravity imposes long-term periodic perturbations onto the CR3BP describing the Earth-Moon system. Therefore, the SBCM may have different canonical forms in the coordinate systems S_{S-E+M} and S_{E-M}.

The Hamiltonian for the SBCM is formulated in the coordinate system S_{S-E+M} as:

$$H_1 = \frac{1}{2}\left(p_x^2 + p_y^2 + p_z^2\right) - xp_y + yp_x - \frac{1-\mu_S}{\|\boldsymbol{R}-\boldsymbol{R}_S\|} - \frac{m_E}{\|\boldsymbol{r}-\boldsymbol{r}_E\|} - \frac{m_M}{\|\boldsymbol{r}-\boldsymbol{r}_M\|}. \quad (6)$$

The Hamiltonian for the SBCM is formulated in the coordinate system S_{E-M} as [13]:

$$H_1 = \frac{1}{2}\left(p_x^2 + p_y^2 + p_z^2\right) - xp_y + yp_x - \frac{1-\mu}{\|\boldsymbol{r}-\boldsymbol{r}_E\|} - \frac{\mu}{\|\boldsymbol{r}-\boldsymbol{r}_M\|} - \frac{m_S}{\|\boldsymbol{R}-a_S\boldsymbol{R}_S\|} - \omega_S^2 \boldsymbol{A}_S^T \boldsymbol{R}_x(-i)\boldsymbol{R}_z(-\beta)\boldsymbol{r} + \frac{m_S}{a_S}, \quad (7)$$

where $\boldsymbol{r}$ and $\boldsymbol{R}$ are the position vector of the spacecraft in S_{E-M} and S_{S-E+M}, respectively; ω_S is the angular velocity of the Earth/Moon system with respect to the inertial reference system; i is the inclination between the lunar and ecliptic planes; μ is the mass ratio of the Moon with respect to the Earth/Moon system; μ_S is the mass ratio of the Earth/Moon system with respect to the full Sun-Earth/Moon system; m_E and m_M are the masses of the Earth and Moon, respectively, and are related as $m_E + m_M = \mu_S$; $\boldsymbol{A}_S = [a_S\cos\theta_S, a_S\sin\theta_S, 0]^T$ is the position vector of the Sun; a_S is the mean distance between the heliocenter and the centroid of the Earth/Moon system; θ_S and β are the solar and lunar phase angles, respectively; $r = [x, y, z]^T$ is the position vector of the spacecraft projected in the SCSEM; and $\boldsymbol{R}_x$ as well as $\boldsymbol{R}_z$ are the element transformation matrices rotating around the x and z axes, respectively.

The initial parameters for the SBCM are set as $\theta_{S0} = 0^0$ ($t_0 = 0$), and β_0 is determined by the relative phases of the Sun, the Earth, and the Moon.

The dynamical model $SBCM_{E-M}$ in the coordinate system S_{E-M} is integrated using the normalized units of the Earth/Moon system as $L_{S-E+M} = 3.84401 \times 10^8$ m, $T_{S-E+M} = 2\pi$ /month, and $M_{S-E+M} = 5.976 \times 10^{24}$ kg. The purpose is to improve the computational efficiency when the evolutions of the invariant manifolds of Halo orbit under lunar gravity are investigated.

2 SITs in the CR3BP

For the stable and unstable manifold theorems of periodic orbits [14], an open subset $\boldsymbol{E} \subset \boldsymbol{R}^n$ contains a periodic orbit $\boldsymbol{\Gamma}: \boldsymbol{x} = \boldsymbol{P}(t)$. If the characteristic exponents of $\boldsymbol{P}(t)$ have a $0 \leqslant k \leqslant n-1$ modulus less than 1, i.e., $|\lambda_j| < 1$, $j = 1, \cdots, k$, and other exponents have a modulus greater than 1, i.e., $|\lambda_j| > 1, j = k+1, \cdots, n-1$, then there is a neighborhood $\boldsymbol{N} \subset \boldsymbol{R}^n$ near any point $\boldsymbol{p} \in \boldsymbol{\Gamma}$. In this neighborhood, the stable manifold $S_\Gamma = \left\{\boldsymbol{x} \in \boldsymbol{N} \middle| d\left(\boldsymbol{\varphi}(t, \boldsymbol{x}), \boldsymbol{\Gamma}\right) \to 0,\ t \to +\infty\right\}$ is a $(k+1)$-dimensional differentiable manifold invariant under the flow $\boldsymbol{\varphi}$. On the other hand, the unstable manifold $N_\Gamma = \left\{x \in \boldsymbol{N} \middle| d\left(\boldsymbol{\varphi}(t, x), \boldsymbol{\Gamma}\right) \to 0, t \to -\infty\right\}$ is a $(n-k)$-dimensional differentiable manifold. The stable and unstable manifolds of $\boldsymbol{\Gamma}$ transversally intersect in $\boldsymbol{\Gamma}$, i.e., $S_\Gamma \bigcap N_\Gamma = \boldsymbol{\Gamma}$.

The symplectic matrix $\boldsymbol{\Phi}$ has the real eigenvalues $\lambda_5 > 1$ and $\lambda_6 < 1$, suggesting that the Halo orbit has both stable and unstable manifolds. Each of these manifolds is a 2-dimensional compact manifold. Its projection is on the position space $\boldsymbol{R}^3$, as shown in Figure 4. The length unit L_{S-E+M} is defined as the average distance between the Sun and the Earth/Moon system.

The stable manifold has a significant application in the design of the transfer trajectories to the Halo orbit [5]. The dynamical behavior of a stable manifold near the Earth can be investigated from another Poincaré map defined by the Poincaré section $\left(\boldsymbol{r} - \boldsymbol{r}_E\right)^T \cdot \boldsymbol{v} = 0$. This section is a mapping of the 2-dimensional stable manifold into a 1-dimensional curve. The map can be expressed by the phasic angle of Halo orbit and the altitude of the perigee (shown in Figure 5).

Table 1 shows all launch locations satisfying no-cost insertion into the Halo orbit distributed within the perigee distance from the ground (200 km at A, B, C, D, E, and F, respectively). The launch velocities and orbital altitudes of the parking orbit in the inertial coordinate system GI, the phasic angles of Halo orbit, and the flight durations are also shown therein. The 3-dimensional representation of SITs in the CR3BP is shown in Figure 6.

Figure 5 demonstrates the geometrical properties of the stable manifolds integrating in a negative time arrow. The curve changes at C, D, E, and F are more dramatic than those at A and B. From the view of a dynamical system integrating in the positive time arrow, the trajectories allocated by A and B are quite sensitive to the initial values in

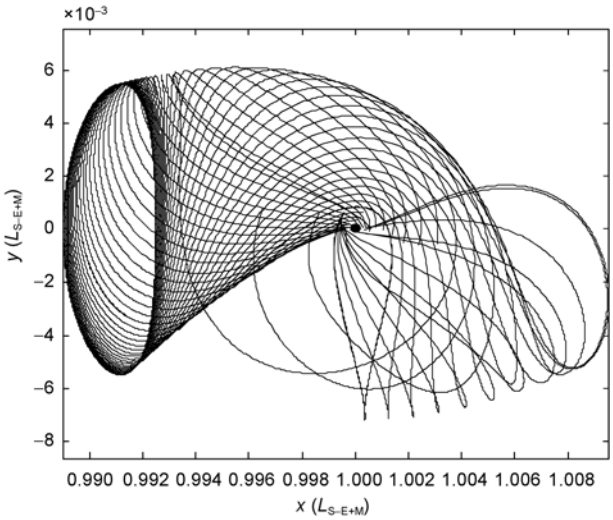

Figure 4 Stable manifold of the Halo orbit on the x-y position space.

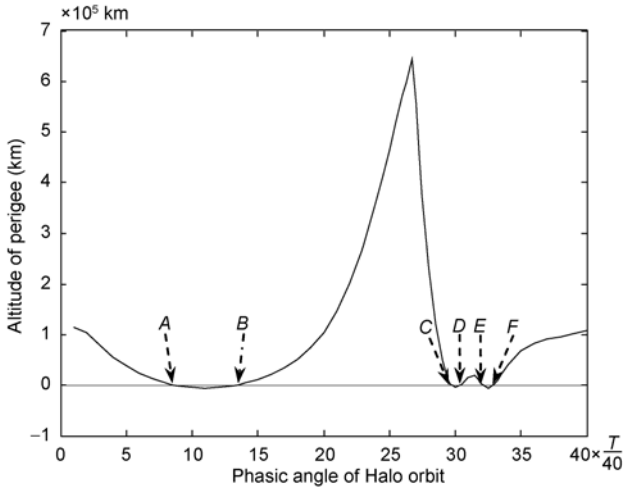

Figure 5 Poincaré section map of the stable manifold of Halo orbit.

the perigree altitudes, compared with those by C, D, and F. The sensitivity is due to the continuities of the solutions to the CR3BP with respect to the initial values [9,15].

3 Low-thrust trajectories transferring to Halo orbits

The following is the design methodology for low-thrust transfer trajectories to Halo orbits. The spacecraft initially increases its Jacobi energy by the long-term effects of the low-thrust propulsion to acquire enough energy for escaping Earth's gravity. The stable manifolds are then inserted after reaching the appropriate velocities to free-fly along the invariant manifolds into the Halo orbit. Previous research on low-thrust propulsion, such as the ION engine [8,10] and

Table 1 Properties of single-impulse transfer trajectories

Case	ΔV (km/s)	Altitude of parking orbit (km)	Phasic angle of Halo orbit (τ)	Flight duration (Month)
A	3.2188	182	0.2193	8.7232
B	3.2147	199	0.3337	8.8932
C	3.2145	201	0.7433	12.3488
D	3.2146	198	0.7599	12.7949
E	3.2144	201	0.8025	12.9783
F	3.2141	199	0.8224	12.4347

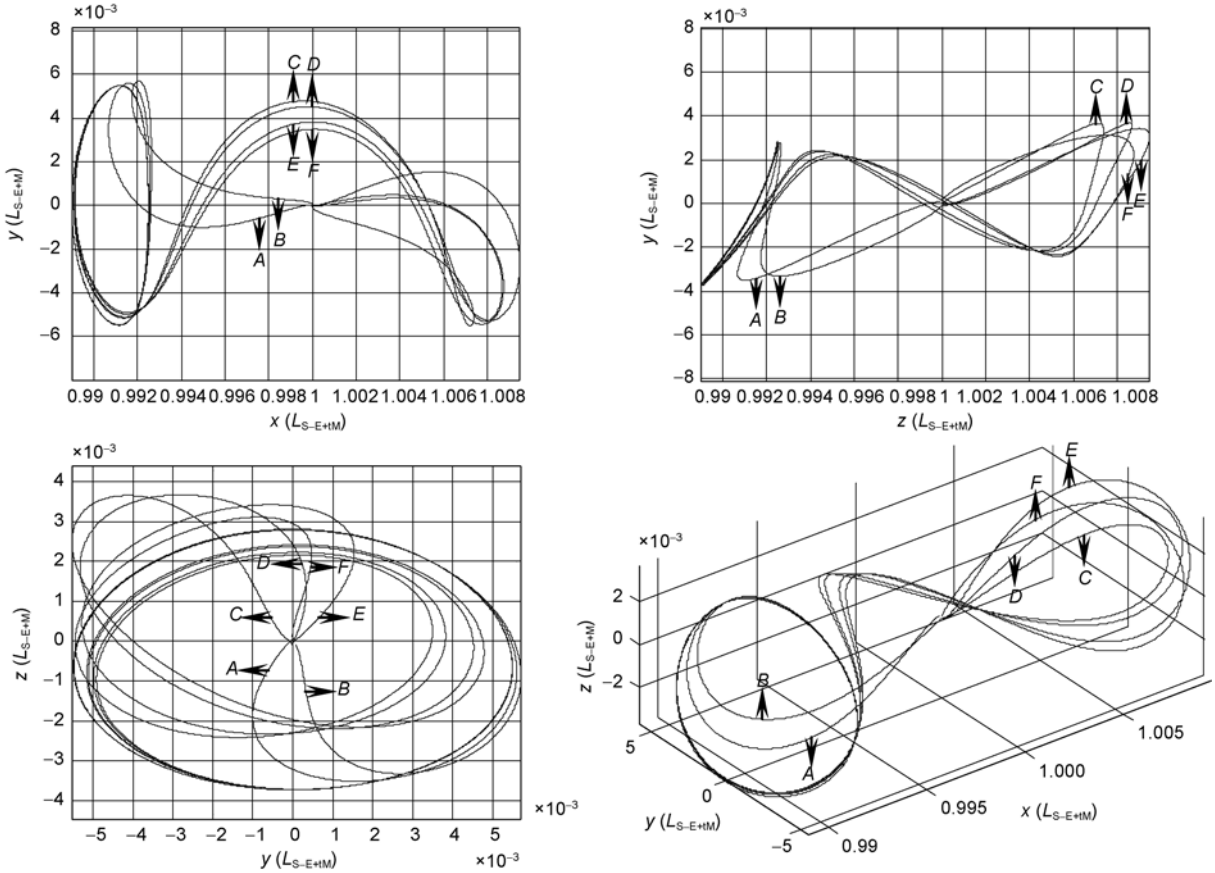

Figure 6 Three-dimensional representation of single-impulse trajectories in the CR3BP.

solar sail [11], focused on guidance laws to escape from the Earth [10,11]. However, the open problem of whether all invariant manifolds can be applied in the design of low-thrust transferring trajectories has not yet been addressed.

Low-thrust acceleration or deceleration does not preserve the Jacobi energy:

$$\dot{C} = -2\boldsymbol{a}\cdot\dot{\boldsymbol{R}}, \tag{8}$$

where C is the Jacobi energy, $\boldsymbol{a}$ is the acceleration or deceleration generated by the low-thrust propulsion, and $\dot{\boldsymbol{R}}$ is the velocity vector of the spacecraft in the frame of S_{S-E+M}.

The control law for low-thrust propulsion is defined from the view of local optimization. The spacecraft has an extremal increase in Jacobi energy when $\boldsymbol{a}$ has the same direction as the velocity vector $\dot{\boldsymbol{R}}$, and *vice versa*. However, this control law does not endow global optimization, which depends on path planning for flight directions. The section overcomes this general difficulty via the local optimal control law, instead of the global optimization for a turning off/on schedule and flight directions, whether all the invariant manifolds can be applied to the design of low-thrust transferring trajectories.

The ION engine excellently performs in high-specific impulse and continuous propulsion in spite of low thrust that a spacecraft has significant reduction in its mass. The spacecraft developed for the lunar mission, SMART-1, has an assembled PPS-1350 Hall (ION) engine. The gas jetting velocity of the engine is 16.434 km/s, and the thrust is 73.19 mN. The total mass is 350 kg, including fuel mass of 74.994 kg. This low-thrust engine undergoes fewer changes in acceleration or deceleration during the flight of a spacecraft. So the ION engine is implemented as the average thrust of SMART-1, $a_0 = 2.3421\times10^{-4}\,\mathrm{m/s^2}$, and fuel reduction and constant thrust in the engine is ignored in this section.

By integration from the negative time arrow, low-thrust trajectories decelerate from high-energy (i.e., Halo orbits) to low-energy (i.e., gravity trap around Earth) regions. Decelerating trajectories are inserted into Halo orbits from the inverse transformation of Γ_1, which is deduced from the dynamical symmetry in the CR3BP, $\Gamma_1 : \tau = -t, Y = -y$.

Based on the control law aforementioned, the dynamical model for low-thrust propulsion in the CR3BP is described as:

$$\begin{cases} \ddot{x} - 2\dot{y} = x - \dfrac{(1-\mu)(x+\mu)}{r_1^3} - \dfrac{\mu(x+\mu-1)}{r_2^3} \\ \qquad\qquad - \dfrac{\dot{x}}{\sqrt{\dot{x}^2+\dot{y}^2+\dot{z}^2}}\cdot a, \\ \ddot{y} + 2\dot{x} = y - \left(\dfrac{1-\mu}{r_1^3} + \dfrac{\mu}{r_2^3}\right) y - \dfrac{\dot{y}}{\sqrt{\dot{x}^2+\dot{y}^2+\dot{z}^2}}\cdot a, \\ \ddot{z} = -\left(\dfrac{1-\mu}{r_1^3} + \dfrac{\mu}{r_2^3}\right) z - \dfrac{\dot{z}}{\sqrt{\dot{x}^2+\dot{y}^2+\dot{z}^2}}\cdot a, \end{cases} \tag{9}$$

where the control law is defined as:

$$a = \begin{cases} a_0, \sqrt{\dot{x}^2+\dot{y}^2+\dot{z}^2} \neq 0, \\ 0, \sqrt{\dot{x}^2+\dot{y}^2+\dot{z}^2} = 0. \end{cases}$$

In other words, the low-thrust propulsion is turned off only when the spacecraft has the velocity $\dot{\boldsymbol{R}}$ of $\mathbf{0}$ in the frame of S_{S-E+M}.

Obviously, the dynamical system (9) has no Hamiltonian structure, whose topology is modified from conservative to dissipative systems. The topologies of the libration points $L_i, i = 1,\cdots,5$ in the CR3BP are degenerated from hyperbolic to asymptotically stable equilibria. The gravity traps of the Sun and the Earth scale the infinite Jacobi energy C. The ultimate destination of a spacecraft stays at the equilibrium $L_i, i = 1,\cdots,5,$ or in the gravity traps around the Sun and the Earth.

The motions near the equilibrium $L_i, i = 1,\cdots,5$ are represented by the following linear model:

$$\begin{cases} \Delta\ddot{x} - 2\Delta\dot{y} + \Omega_{xx}\Delta x + \Omega_{xy}\Delta y = -\dfrac{\Delta\dot{x}}{v}a, \\ \Delta\ddot{y} + 2\Delta\dot{x} + +\Omega_{xy}\Delta x + \Omega_{yy}\Delta y = -\dfrac{\Delta\dot{y}}{v}a, \\ \Delta\ddot{z} + \Omega_{zz}\Delta z = -\dfrac{\Delta\dot{z}}{v}a, \end{cases} \tag{10}$$

where v is the relative velocity with respect to equilibrium, $v = \sqrt{\Delta\dot{x}^2+\Delta\dot{y}^2+\Delta\dot{z}^2} = \sqrt{\dot{x}^2+\dot{y}^2+\dot{z}^2}$; and Ω_{kl} is the second-order partial derivative of the pseudo-potential function Ω with respect to k and l, $(k,l) = (x,y,z)$.

The relative position and velocity $[\Delta x\ \Delta y\ \Delta z\ \Delta\dot{x}\ \Delta\dot{y}\ \Delta\dot{z}]^{\mathrm{T}}$ approach zero when the spacecraft has access to the equilibrium. However, the relative acceleration or deceleration remains at a constant a_0:

$$\Delta\ddot{\boldsymbol{R}} = \boldsymbol{a} + O\left(\boldsymbol{R}, \dot{\boldsymbol{R}}\right). \tag{11}$$

The spacecraft moves in an opposite direction to the velocity vector $\dot{\boldsymbol{R}}$, and $a_0 \gg O\left(\|\boldsymbol{R}\|, \|\dot{\boldsymbol{R}}\|\right)$. Hence, the spacecraft may find its equilibrium within limited time. In other words, the oscillations near the equilibrium $L_i, i = 1,...,5$ do not remain stabilized until such limited time is up. However, the duration may last longer.

Figure 7 illustrates the dynamical stabilization by the low-thrust deceleration near EL_1. All motions near EL_1 participate in periodic/quasi-periodic oscillations (i.e., Lyapunov, Halo, or Lissajous orbits), exponentially converging or diverging in position space (i.e., the stable and unstable manifolds). Therefore, low-thrust propulsion does not only eliminate divergent trends in an unstable manifold, but also

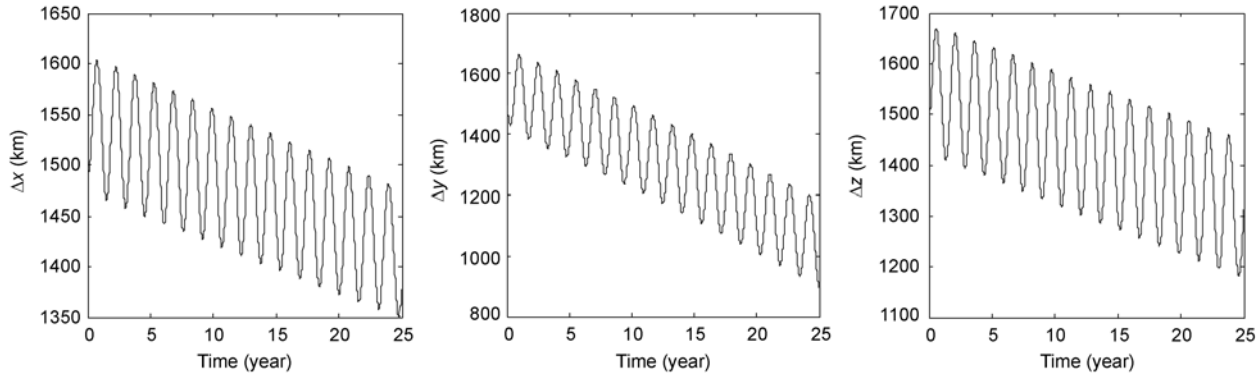

Figure 7 Stabilization near EL_1 by low-thrust deceleration.

endows asymptotical stability.

The boundaries of the gravity traps of the Sun and the Earth are defined as zero velocity surfaces near EL_1, i.e., $M=\left\{(x,y,z)\middle|2\Omega(x,y,z)+C_{EL_1}=0\right\}$. Hence, the different traps are separated by EL_1: when the spacecraft has less Jacobi energy than EL_1, there are transiting trajectories between the two gravity traps; when the spacecraft has more Jacobi energy than EL_1, the trajectories are restricted inside the boundaries of the gravity traps, without any transit occurring between the two traps. Hence, the spacecraft can be treated as a satellite or asteroid orbiting the Sun or Earth.

Actually, the trajectory acceleration or deceleration implemented by low-thrust propulsion is similar to the LEO satellite, with its opposite direction to the relative velocity between the satellite and atmospheric drag. This phenomenon is referred to as the famous aerodynamic paradox. The deceleration implemented by the atmospheric drag causes an increase in the velocity of the satellite. The paradox occurs in the phase of the low-thrust deceleration implemented in the gravity trap of the Earth, instead of the transit phase between the gravity traps of the Earth and the Sun.

With the stabilization for phasic angle 0 on the Halo orbit at EL_1, inefficient deceleration is implemented by the low-thrust propulsion near a libration point. The inefficiency is attributed to the fact that a spacecraft snails from location × to location ∗ (Figure 8) for one year (i.e., $2\pi T_{\mathrm{S-E+M}}$). The extremely slow movement of a spacecraft near EL_1 is caused by the decrease in the velocity of the spacecraft in the frame of $\mathrm{S_{S-E+M}}$ due to low-thrust deceleration. Therefore, the paradox enhancing the velocity is replaced by the phenomenon stagnating near a libration point, as implemented by the low-thrust propulsion. Figure 9 illustrates the velocity history of stabilization by low-thrust deceleration. The spacecraft damps its velocity up to 0.0402 m/s in a very short period of time (around $0.2496T_{\mathrm{S-E+M}}$), and then keeps a small oscillation in the vicinity of Location ∗.

The low-thrust propulsion near a libration point is too inefficient to have any engineering application in acceleration or deceleration. So a spacecraft is expected to free-fly along

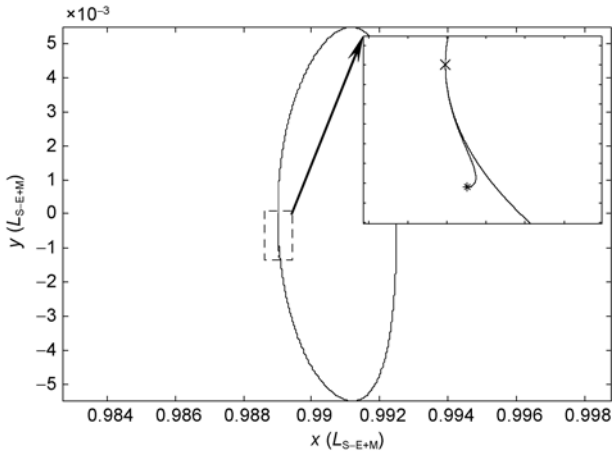

Figure 8 Stabilization of the phasic angle 0 on the Halo orbit at EL_1 by low-thrust deceleration.

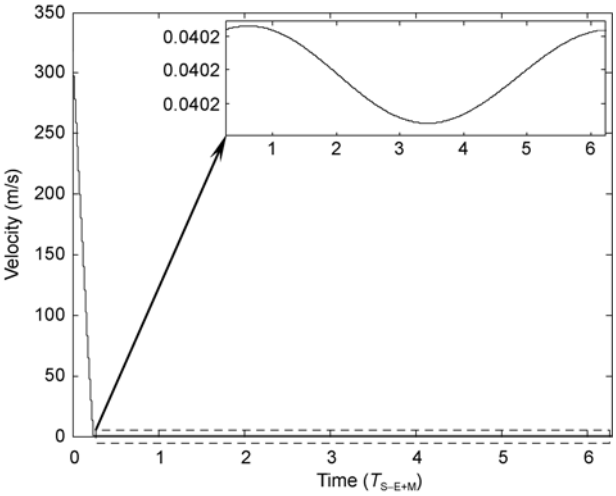

Figure 9 Velocity history of stabilization by low-thrust deceleration.

the stable manifolds $W^{S}_{\mathrm{E+M}}$ to increase its velocity and avoid stagnation near a libration point. This phenomenon explains the selection of the invariant manifolds as the entrance for transferring to the Halo orbit, rather than the

nominal orbit itself.

A turning on/off schedule for low-thrust propulsion is introduced for the controlled manifolds avoiding stagnation on libration points. Too early booting does not make the spacecraft accumulate enough velocity to avoid stagnation. Too late booting may not enable the spacecraft to be captured by Earth. The dynamical system (7) or (9) describing the low-thrust propulsion in the CR3BP is an autonomous dissipative system. No time node is available to measure the booting schedule. Hence, the length of the interception distance along the x axis is introduced to measure the schedule. All the invariant manifolds beyond the interception are referred to as controlled manifolds booted by the low-thrust propulsion.

The turning on/off schedule and earliest booting time measured by the interception distance along the x axis depend on the stagnating duration accepted by the authors. Therefore, the booting time is only the accepted earliest time, not the real earliest one.

The stagnating trajectories defined in the present paper, are those generated from integrating the dynamical equations at the step of $(1\times10^{-4})T_{\text{S–E+M}}$ by the Dormand–Prince algorithm. This algorithm is integrated using the tool ODE5 by the software Simulink4.0®, with an integration period of more than 5 min (physical time). The hardware platform is Intel(R) Core(TM) 6300@1.86GHz CPU and 1G RAM. The accepted earliest booting time defines the lengths of the controlled manifolds, which is measured by the interception distance along the x axis in Figure 10. Obviously, all the stagnating trajectories by the low-thrust propulsion reducing the Jacobi energy from C_{Halo} (Jacobi energy on the Halo orbit and its invariant manifolds) to C_{EL_1} (Jacobi energy at EL_1), have been ignored when the accepted earliest booting time is counted for controlled manifolds.

The spacecraft has reduced its Jacobi energy up to C_{EL_1} at EL_1 by the accepted earliest booting time and low-thrust propulsion. However, the spacecraft still has the opportunity to stay away form EL_1. Therefore, the endings of the controlled manifolds lying inside the boundary of the Earth's gravity trap in the configuration space need to be investigated. Figure 11 depicts all the controlled manifolds in the configuration space with their Jacobi energy reduced from C_{Halo} to C_{EL_1}. Figure 12 presents the uncontrolled trajectories after the Jacobi energy is reduced to C_{EL_1}, and then the low-thrust propulsion is removed.

Figure 11 indicates that all the endings of controlled manifolds lie inside the boundary of the Earth's gravity trap in the configuration space. Figure 12 indicates that all uncontrolled trajectories, after their Jacobi energy is reduced to C_{EL_1}, are restricted inside the boundaries of gravity traps without any transit occurring between the traps.

Hence, the solution to the open problem is that all controlled manifolds need to be captured inside the boundary of Earth's gravity trap. All invariant manifolds can also be

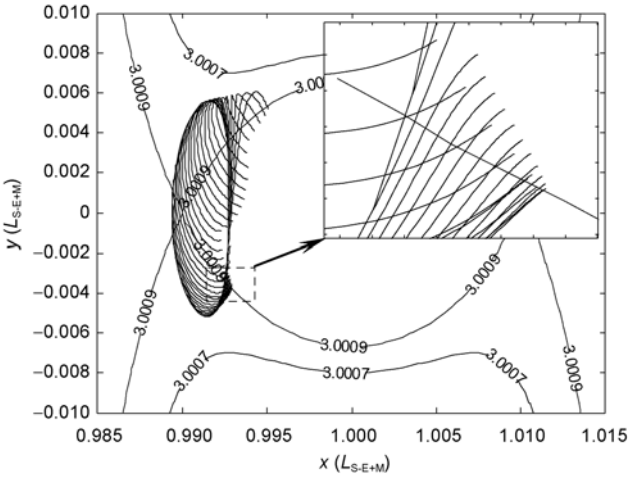

Figure 11 Controlled manifolds in the configuration space with their Jacobi Energy reduced to C_{EL_1}.

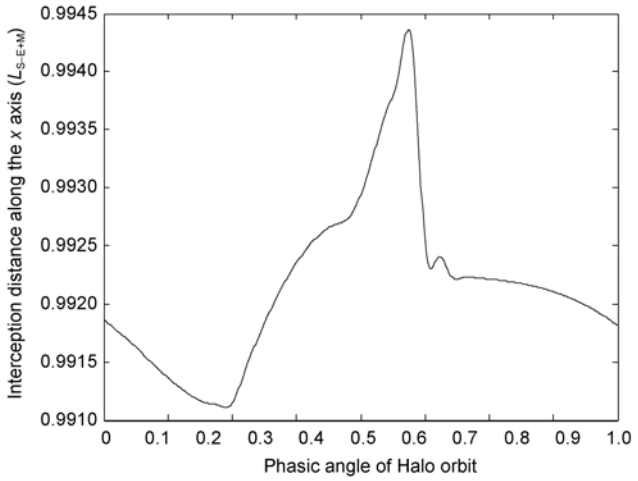

Figure 10 Accepted earliest booting time defined by the Jacobi energy at EL_1.

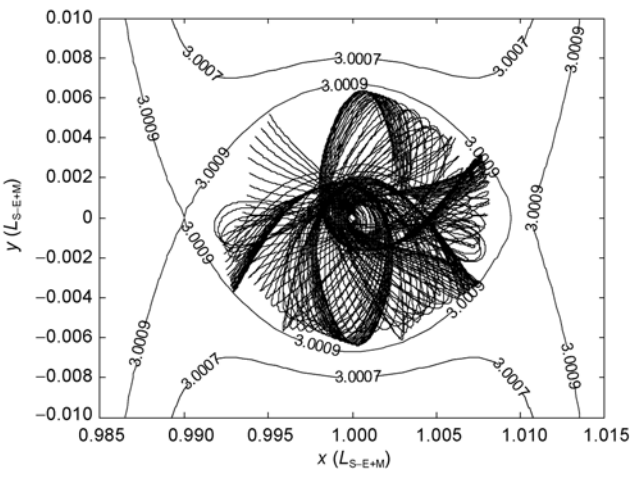

Figure 12 Uncontrolled trajectories after the Jacobi Energy is reduced to C_{EL_1} and then the thrust is removed.

applied to design low-thrust transferring trajectories.

4 SITs in the SBCM

In the absence of perturbations, a spacecraft may take infinite time to insert into or escape from Halo orbits along invariant manifolds. However, the periodic perturbation imposing on the SBCM model from lunar gravity may destroy the closed forms of Halo orbits at EL_1 or EL_2. The perturbation may also drive any point in the Halo orbit to depart from the nominal orbit without maneuvers within a finite time.

Some optimizations on lunar flyby trajectories to Halo orbits have been developed [9]. However, some difficult problems remain, such as the existence of single-impulse trajectories surviving the lunar perturbation. The Lebesgue measure of invariant manifolds preserving the topologies in the CR3BP under the perturbation is also a problem. Some branches of the stable manifolds are integrated into the gravity trap of the Earth from the negative time arrow. These branches are referred to as SITs transferring to Halo orbits.

4.1 SITs from the earth to Halo orbits

The dynamical model $\mathrm{SBCM_{E-M}}$ is integrated into the coordinate system $\mathrm{S_{E-M}}$ to investigate the evolutions of the invariant manifolds of Halo orbit under lunar gravity [16]. Figure 13 shows the ergodic surveys on the parameters of the perigee altitudes, phasic angles of the Halo orbit, and relative phases of the Sun, the Earth, and the Moon. These surveys act as the initial guess to generate the real transfer trajectories to the Halo orbit in the ephemeris model from the iterative routine.

Based on the evolutions of invariant manifolds, most of them have preserved their topologies in the CR3BP. There are also slight changes in the relationship between the perigee altitudes and lunar phase angle β. β is used to generate the SITs from the Earth or the Moon to Halo orbits. The perigee altitudes of few manifolds are quite non-continuous with the lunar phase angles, which can be utilized to generate single-impulse lunar flyby trajectories.

Three types of flyby trajectories marked as ■, ▲, and ● are displayed in Figure 14. Their orbital elements (semi-major axis and eccentricity) in the inertial frame of GI are shown in Figures 15, 16, and 17. Types ■, ▲, and ● have the common features of the flyby trajectories in numerical jumps in orbital elements at $-136.6T_{\mathrm{E+M}}$ (■), $-137.4T_{\mathrm{E+M}}$ (▲), and $-253.5T_{\mathrm{E+M}}$ (●).

Type ■ decreases its semi-major axis or Jacobi energy when the trajectory is approaching lunar gravity, which is undesirable. However, types ▲ and ● increase their semi-major axes or energies when the trajectories are approaching the Moon, which is preferred for transferring to Halo orbits.

4.2 SITs from the moon to Halo orbits

The dynamical model $\mathrm{SBCM_{E-M}}$ is integrated in the coordinate system $\mathrm{S_{E-M}}$ from the invariant manifolds of a Halo orbit at EL_2 to the Poincaré section $\Sigma: r^{\mathrm{T}}\dot{r}=0$. The purpose is to investigate the evolutions of the invariant manifolds of a Halo orbit under lunar gravity, and to generate SITs from the Moon to Halo orbits.

The spacecraft parking on the lunar pole orbit with an altitude of 100 km needs at least 3 maneuvers to insert into the stable manifolds of Halo orbits. The first maneuver ΔV_1 is used to raise the altitude of apolune. The second maneuver ΔV_2 is used to change its inclination and RAAN. The

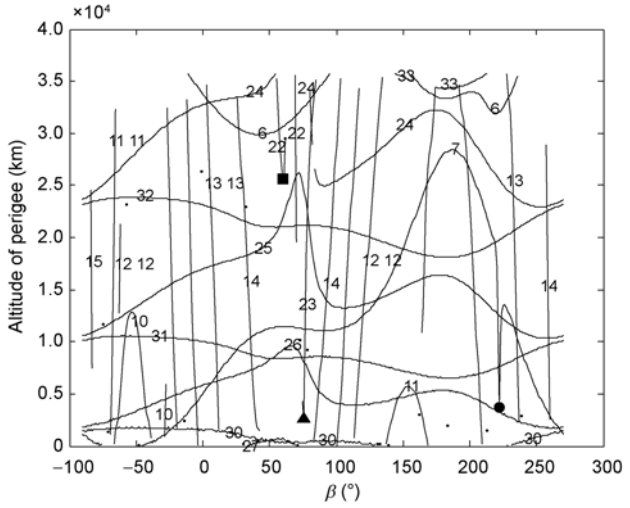

Figure 13 Ergodic survey of the parameters of perigee altitudes, phasic angles of the Halo orbit, as well as relative phases of the Sun, the Earth, and the Moon (Arabic numbers are marked as 40τ, measuring the phasic angles of Halo orbit).

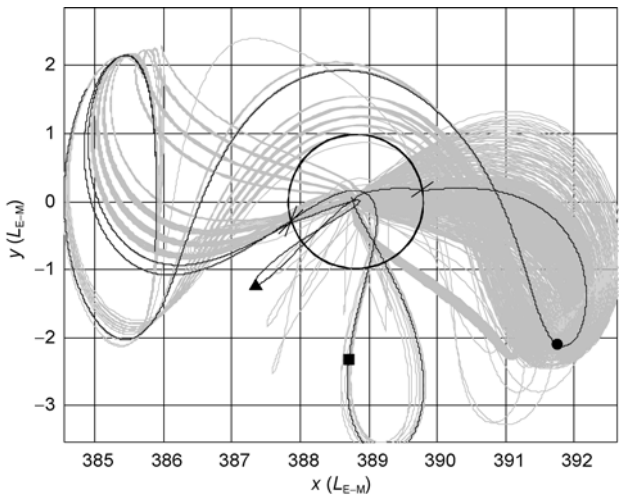

Figure 14 All simple-impulse transfer trajectories to the Halo orbit at EL_1 in the SBCM.

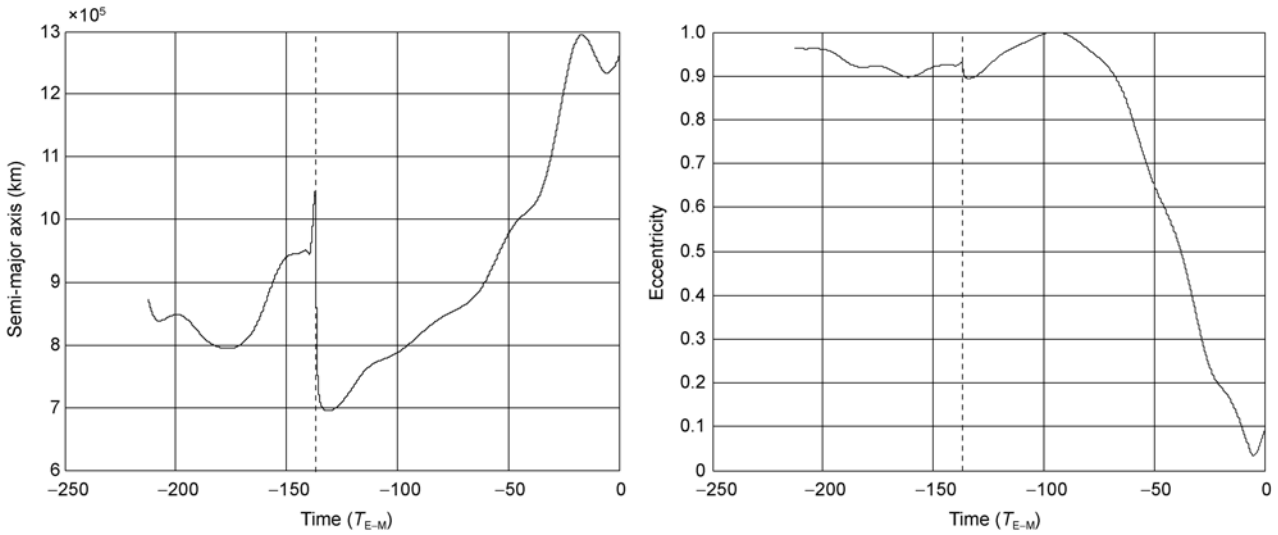

Figure 15 Histories of the semi-major axis and eccentricity for type ■ of flyby trajectories.

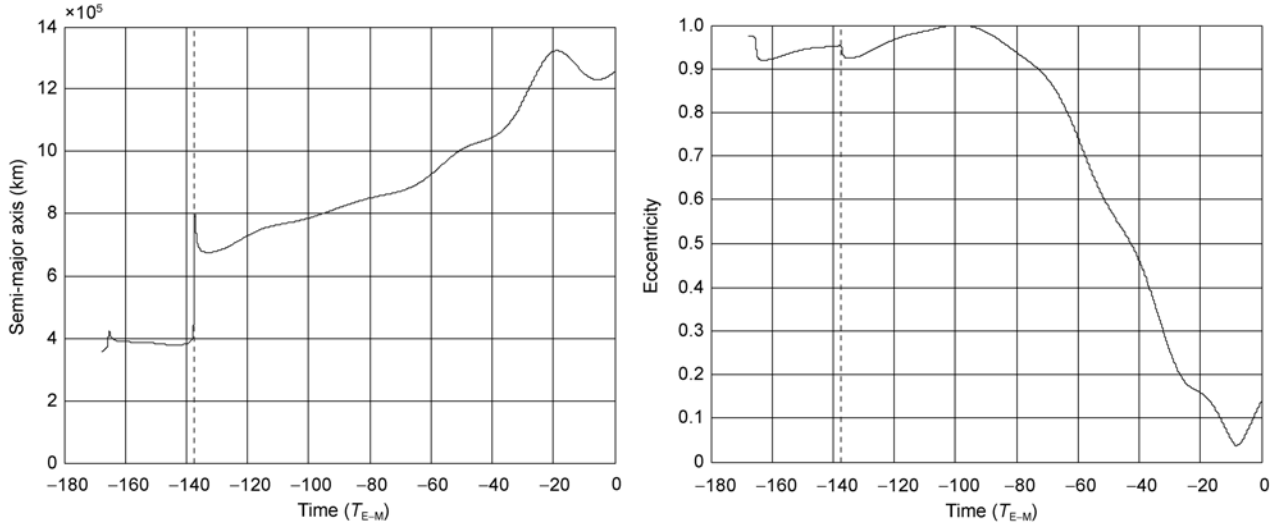

Figure 16 Histories of the semi-major axis and eccentricity for type ▲ of flyby trajectories.

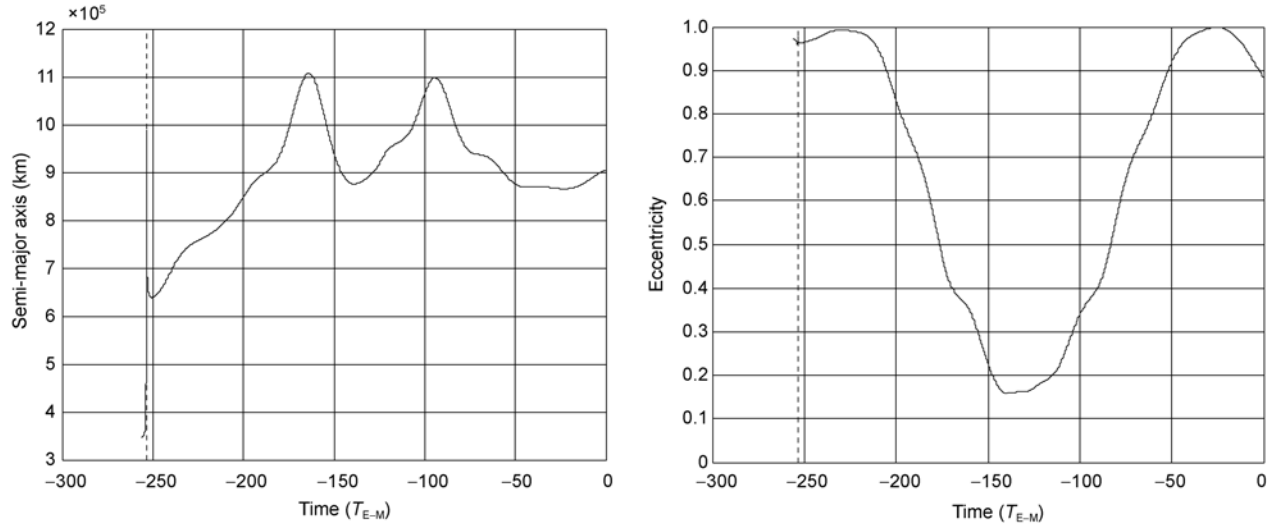

Figure 17 Histories of the semi-major axis and eccentricity for type ● of flyby trajectories.

third maneuver ΔV_3 is driving the spacecraft to free-fly along the SIT. The transferring windows and properties of SITs from lunar pole orbits are demonstrated respectively in Figure 18 and Table 2.

Transferring windows are defined as angle intervals of the relative phase β of the Sun, the Earth, and the Moon. During these windows, invariant manifolds have a distance less than 62636 km (the radius of the lunar gravitational sphere of influence) from the lunar surface. The SITs lie on the angle intervals as [54°, 64°], [120°, 126°], [138°, 140°], [144°, 146°], [288°, 290°], and [352°, 356°]. Their representations in the position space are demonstrated in Figures 19 and 20. The most economical trajectory with its ΔV around 1000m/s occurs at the relative angle β of 354° belonging to the interval [352°, 356°], depicted by the most thick solid lines in Figures 19 and 20.

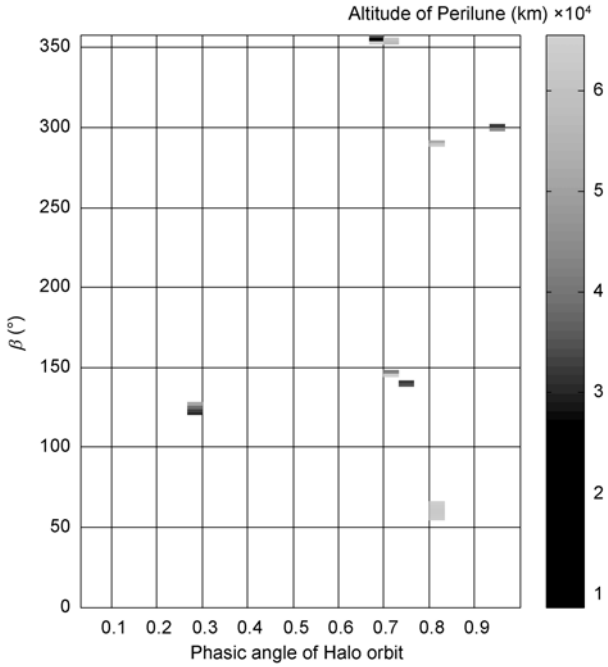

Figure 18 Transferring windows of single-impulse trajectories from lunar pole obits.

5 Conclusions

The evolutions of the invariant manifolds of Halo orbits are investigated in CR3BP and SBCM. The possible application of these manifolds in designing low-thrust transferring trajectories, and the presence of SITs under lunar gravity are explained. The relationship between the invariant manifolds and the perigee altitude is investigated using a Poincaré map. Six types of SITs are attained from the geometry of the invariant manifolds. The evolutions of the controlled manifolds are indicated by the gradient law of Jacobi energy, and the following conclusions are drawn. First, the low thrust (acceleration or deceleration) near a libration point is very inefficient that a spacecraft free-flies along the invariant

Table 2 Properties of single-impulse transfer trajectories from the Moon to the Halo orbit

β (°)	Phasic angle of a Halo orbit (τ)	Altitude of parking orbit (km)	Inclination (°)	$\Delta V_1 + \Delta V_2 + \Delta V_3$ (m/s)	Flight duration (day)
54	24	6700	38.328	1532.1	91.12
56	24	65603	41.008	1532.1	91.256
58	24	64803	43.447	1532	91.397
60	24	64821	45.51	1531.8	91.55
62	24	65581	47.103	1531.8	91.707
64	24	67026	48.175	1531.4	91.876
120	8	18996	84.043	1114.3	113.94
122	8	27220	86.678	1204.2	114.22
124	8	39223	88.625	1284.6	114.53
126	8	53378	89.987	1338	114.86
138	22	31351	77.099	1238.6	109.51
140	22	25008	116.09	1036.8	110.27
144	21	66616	81.402	1536.9	109.07
146	21	43407	82.306	1431.3	109.57
288	24	65078	119.82	1306.1	122.53
290	24	54017	76.839	1409.7	121.49
298	28	46026	23.136	1570.6	111.13
300	28	25517	157.44	1316.5	110.58
352	20	66591	122.96	1306.2	98.295
352	21	59589	102.66	1220.7	98.888
354	20	10471	115.53	1005.9	97.817
354	21	63614	83.541	1287.7	98.398
356	20	32647	73.059	1301.7	97.48

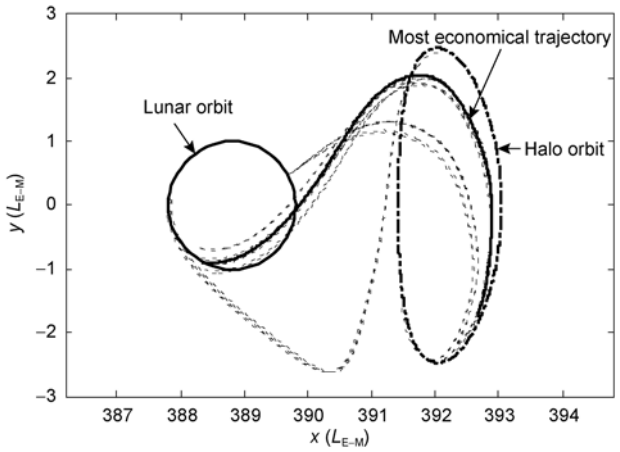

Figure 19 Single-impulse transfer trajectories from lunar pole orbits to the Halo orbit in the Syzygy coordinate system of the Sun-Earth/Moon System.

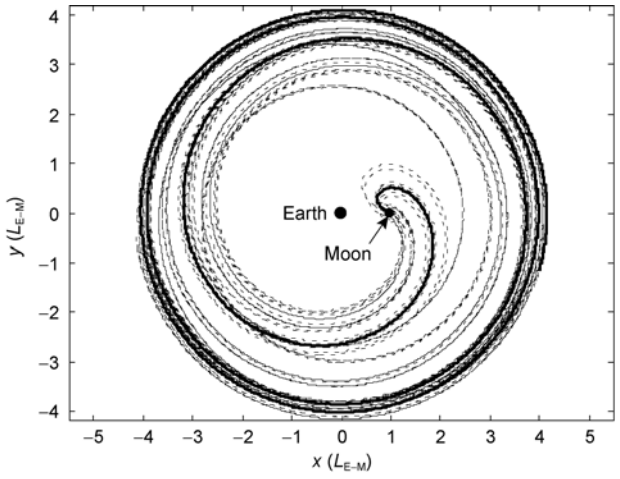

Figure 20 Single-impulse transfer trajectories from lunar pole orbits to the Halo orbit in the Syzygy coordinate system of the Earth-Moon System.

manifolds to increase its velocity and avoid stagnation near the libration point. Second, all the controlled manifolds are captured because they lie inside the boundaries of the gravity traps of the Earth in the configuration space. A turning on/off schedule for low-thrust propulsion is introduced to the controlled manifolds avoiding the stagnation on libration points to measure the interception distance along the x axis. The evolutions of invariant manifolds under lunar gravity are indicated from the relationship between the lunar phasic angle as well as the altitudes of the perigee and perilune. Third and last, most of the manifolds have preserved their topologies in the CR3BP, which are used to generate the transfer trajectories from the Earth or Moon to Halo orbits. However, the perigee altitudes of few manifolds are quite non-continuous, which can be used to generate single-impulse flyby trajectories.

The evolutions of the invariant manifolds of a Halo orbit under low-thrust propulsion and lunar gravity are emphasized in the present paper. All invariant manifolds can be applied in designing low-thrust transferring trajectories. There are also remaining SITs preserved under lunar gravity. Trajectories may be constructed from ergodic surveys of the parameters of the phasic angles of a Halo orbit and relative phases of the Sun, the Earth, and the Moon. The constructed trajectories act as an initial guess to generate the real transfer trajectories to the Halo orbit in the ephemeris model from the iterative routine.

This work was supported by the National Natural Science Foundation of China (Grant No. 11172020), the "Vision" Foundation for the Talents from Ministry of Industry and Information Technology of China, and the "BlueSky" Foundation for the Talents from Beijing University of Aeronautics and Astronautics.

1 Xu M, Xu S J. The application of libration points and Halo orbits in the Earth-Moon system to space mission design (in Chinese). Chin J Astronaut, 2006, 27(4): 695–699
2 Xu S J, Xu M. A new constellation configuration scheme for communicating architecture in cislunar space. In: 57th International Astronautical Congress. Valencia, Spain, 2006. IAC-06-A3.4.03
3 Farquhar R W, Muhonen D P, Newman C, et al. Trajectories and orbital maneuvers for the first libration-point satellite. J Guidance Control Dyn, 1980, 3(6): 549–554
4 Gómez G, Jorba À, Masdemont J, et al. Study of the transfer from the Earth to a Halo orbit around the equilibrium point L_1. Celest Mech Dyn Astron, 1993, 56(4): 541–562
5 Howell K C, Barden B, Lo M W. Application of dynamical systems theory to trajectory design for a libration point mission. J Astronaut Sci, 1997, 54(2): 161–178
6 Xu M, Xu S J. Trajectory and correction maneuver during the transfer from Earth to Halo orbit. Chin J Aeronaut, 2008, 21(3): 200–206
7 Xu M, Xu S J. Low-energy trajectory from Earth to Moon for low-thrust spacecraft (in Chinese). Acta Aeronaut Astronaut Sin, 2008, 29(4): 781–787
8 Ozimek M T, Howell K C. Low-thrust transfers in the Earth–Moon system, including applications to libration point orbits. J Guidance Control Dyn, 2010, 33(2): 201–207
9 Wilson R S, Howell K C. Trajectory design in the Sun-Earth-Moon system using multiple lunar gravity assists. J Spacecraft Rockets, 1998, 35(2): 191–198
10 Ren Y, Cui P Y, Luan E J. Study of low-thrust transfer to Halo Orbit with invariant manifolds (in Chinese). J Astronaut, 2007, 28(5): 1113–1118
11 Qin J F, Baoyin H, Li J F. Optimal trajectory design of solar sail transfer to Halo orbits (in Chinese). J Tsinghua Univ Sci Tech, 2007, 47(6): 1361–1365
12 Richardson D L. Analytical construction of periodic orbits about the collinear points. Celest Mech Dyn Astron, 1980, 22(3): 241–253
13 Xu M. Spacecraft Orbital Dynamics and Control Based on Libration Point Theories (in Chinese). Dissertation for the Doctoral Degree. Beijing: Beijing University of Aeronautics and Astronautics, 2008
14 Howell K C, Beckman M, Patterson C. Representations of invariant manifolds for applications in three-body systems. J Astronaut Sci, 2006, 54(1): 69–93
15 Kechichian J A. Computational aspects of transfer trajectories to Halo orbits. J Guidance Control Dyn, 2001, 24(4): 796–804
16 Xu M, Xu S J. Exploration of distant retrograde orbits around Moon. Acta Astronaut, 2009, 65(5-6): 853–860